Geochemistry Geophysics Geosystems G3

Article
Volume 14, Number 10
18 October 2013
doi: 10.1002/ggge.20278
ISSN: 1525-2027

Published by AGU and the Geochemical Society

Geophysical modeling of collapse-prone zones at Rumble III seamount, southern Pacific Ocean, New Zealand

F. Caratori Tontini and C. E. J. de Ronde
GNS Science, Marine Geoscience, 1 Fairway Drive, Lower Hutt 5010, New Zealand (f.caratori.tontini@gns.cri.nz)

J. C. Kinsey, A. Soule, and D. Yoerger
Woods Hole Oceanographic Institution, Woods Hole, Massachusetts, USA

L. Cocchi
Istituto Nazionale di Geofisica e Vulcanologia, Fezzano, La Spezia, Italy

[1] Catastrophic collapses of submarine volcanoes have the potential to generate major tsunami, threatening many coastal populations. Recognizing the difficulties surrounding anticipations of these events, quantitative assessment of collapse-prone regions based on detailed morphological, geological, and geophysical mapping can still provide important information about the hazards associated with these collapses. Rumble III is one of the shallowest, and largest, submarine volcanoes found along the Kermadec arc, and is both volcanically and hydrothermally active. Previous surveys have delineated major collapse features at Rumble III; based on time-lapse bathymetry, dramatic changes in the volcano morphology have been shown to have occurred over the interval 2007–2009. Furthermore, this volcano is located just ∼300 km from the east coast of the North Island of New Zealand. Here, we present a geophysical model for Rumble III that provides the locations and sizes of potential weak regions of this volcano. Shipborne and near-seafloor geological and geophysical data collected by the AUV *Sentry* are used to determine the subsurface distribution of weak and unstable volcanic rocks. The resulting model provides evidence for potentially unstable areas located in the Southeastern flank of this volcano which should be included in future hazard predictions.

Components: 8,672 words, 6 figures, 1 table.

Keywords: Rumble III; geophysical modeling; flank collapse; AUV mapping.

Index Terms: 3070 Submarine landslides: Marine Geology and Geophysics; 3005 Marine magnetics and paleomagnetics: Marine Geology and Geophysics; 3080 Submergence instruments: ROV, AUV, submersibles: Marine Geology and Geophysics; 3045 Seafloor morphology, geology, and geophysics: Marine Geology and Geophysics.

Received 11 September 2013; **Accepted** 20 September 2013; **Published** 18 October 2013.

Caratori Tontini, F., C. E. J. de Ronde, J. C. Kinsey, A. Soule, D. Yoerger, and L. Cocchi (2013), Geophysical modeling of collapse-prone zones at Rumble III seamount, southern Pacific Ocean, New Zealand, *Geochem. Geophys. Geosyst.*, *14*, 4667–4680, doi:10.1002/ggge.20278.

1. Introduction

[2] Major flank collapses have been observed at more than 200 volcanoes worldwide [*McGuire*, 1996; *Siebert et al*., 1987], and in the case of submarine volcanoes, they may have caused some of the most destructive tsunami events known [*Smith and Shepherd*, 1996; *McGuire*, 2006]. Many of these collapses are coincident with evidence of pressurization of hydrothermal pore fluids, as in the case of phreatic explosions [*Day*, 1996; *Reid*, 2004]. In addition, hydrothermal alteration of volcanic rocks is considered a causative factor for increasing volcano instability [*Reid et al*., 2001; *Lopez and Williams*, 1993]. In some cases, the intrusion of juvenile magma into the edifice may trigger destabilization by increasing the load on the volcano, which then cannot support the edifice, such as in Bezymianny-type collapses [*Siebert et al*., 1987; *Day*, 1996]. In other cases, major failures have occurred without any magmatic intrusion, such as the Bandai-type and Unzen-type collapses [*Siebert et al*., 1987; *Day*, 1996]. This latter kind of failure was characterized by the presence of shallow hydrothermal systems at the time of collapse, but hydrothermally altered rocks were found only in a fraction of the resulting avalanches [*Reid*, 2004].

[3] Numerical modeling of pore-fluid pressurization has shown the potential for this process to destabilize large portions of a volcano [*Reid*, 2004; *Elsworth and Voight*, 1995; *Day*, 1996]. Direct evidence of pore-fluid pressurization has been observed in volcanic systems [*Bjornsson et al*., 1976; *Watanabe*, 1983] and hydrothermal breccias [*Sillitoe*, 1985]. It is also known that hydrothermal alteration has an important role in weakening volcanic rocks because of an effective reduction of the friction coefficients and cohesion parameters [*Jaeger and Cook*, 1979; *Watters and Delahaut*, 1995; *Watters et al*., 2000]; some major flank collapses have also involved hydrothermally altered rocks [*Lopez and Williams*, 1993; *Reid et al*., 2001]. However, if both hydrothermal pore-fluid pressurization and hydrothermal alteration effects are present, the former is considered a more important factor in reducing volcano stability [*Day*, 1996]. Either way, detailed surface topography and subsurface imaging of rock properties, using geophysical methods to map rock density and strength, and the extent and location of any hydrothermal system and associated altered rocks, is of paramount importance when assessing 3-D edifice stability. This information allows estimates of failure locations and expected volumes to be calculated to assess the corresponding hazard.

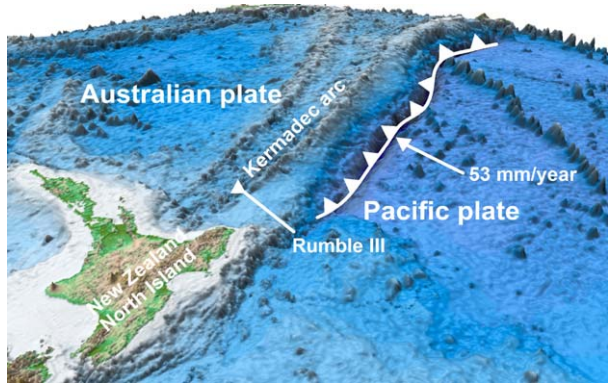

Figure 1. Map showing the main tectonic elements of the region and location of Rumble III volcano. Subduction rate from *DeMets et al*. [2010].

[4] The collapse hazard associated with Rumble III seamount is relevant because of its close proximity to the northeast coast of the North Island of New Zealand (Figure 1). *Latter et al*. [1992] first noted this volcano's tsunami hazard potential. The first dramatic confirmation of Rumble III's volcanic and hydrothermal activity was found in mid-July 1986, when the crew of a Japanese fishing boat reported steam rising from the ocean at 35°44′S, 178°29′E, and a sulfur slick covering an area of 500 m^2. The New Zealand Meteorological office reported a satellite-derived sea surface temperature anomaly of approximately +2° in the area between 10 and 14 July 1986. In the following weeks, discolored water due to a rising gas plume (probably S-rich) [*de Ronde et al*., 2001] was detected above the summit of Rumble III [*Latter et al*., 1992]. There is also direct evidence of significant variations in the shape of the Rumble III edifice from different bathymetric surveys at various times [*Dodge*, 2010].

2. Rumble III: Geological and Geophysical Information

[5] Prior to this study, available information on Rumble III mainly related bathymetric [*Wright*, 1994] and hydrothermal plume surveys [*de Ronde et al*., 2001]. In this section, we review that information and show new data collected during the 2011 NZASMS (New Zealand American *Sentry* Massive Sulfide) cruise. Two dives of the Autonomous Underwater Vehicle (AUV) *Sentry* were dedicated to mapping the summit part of Rumble III. *Sentry* was equipped with Conductivity,

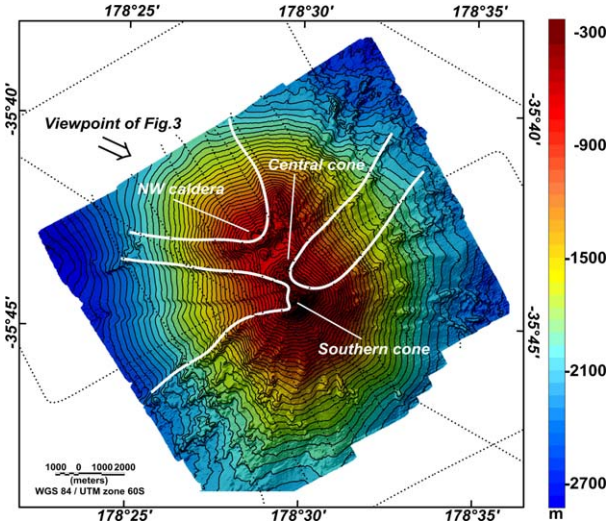

Figure 2. Rumble III EM302 bathymetry (25 m resolution). Contour lines every 50 m. White lines represent the shape and locations of past flank failures. The black dotted lines represent the shipborne geophysics survey lines.

Temperature, and Depth (CTD) and optical backscatter, pH and Eh (redox) sensors, a sidescan sonar and fluxgate magnetometers. In addition, plume mapping and towed camera data, and surface-derived multibeam, gravity and magnetic data also were collected while aboard the R/V Tangaroa.

2.1. Tectonic, Geological, and Morphological Setting

[6] Rumble III is one of many submarine volcanoes along the 2500 km long Kermadec intraoceanic arc (Figure 1), formed by westward subduction of the Pacific Plate under the Australian Plate [*Wright*, 1994; *de Ronde et al*., 2001]. With a constructional volume of 260 km^3 it is one of the largest active stratovolcanoes in the entire Kermadec arc, with a basal diameter of ~25 km at a water depth of ~2500 m and a summit rising to within ~200 m of the sea surface (Figure 2) [*Wright*, 1994; *Wright et al*., 2002].

[7] Like many other volcanoes along the Kermadec arc, Rumble III is host to strong seafloor hydrothermal activity, as determined by plume mapping, and widespread zones of hydrothermally altered rocks have been observed [*de Ronde et al*., 2001]. The hydrothermal plumes of Rumble III are extremely rich in magmatic volatiles and dissolved Fe and Mn, with a large ^{3}He anomaly, a clear marker of hydrothermal activity [*de Ronde et al*., 2001; *Baker et al*., 2003; *Massoth et al*., 2003]. The intense hydrothermal activity at Rumble III suggests that weakening from hydrothermal alteration might be a relevant cause to explain flank collapses.

[8] The volcano morphology, shown by the bathymetry grid (Figures 2 and 3), is characterized by a ~7 km long, northwest striking summit ridge, comprising the southern and central cones and the NW caldera. The southern cone has a circular top, shoaling to ~230 m water depth. The NW caldera has a ~800 m diameter circular shape, with ~100–200 m high walls. The central cone, with a more irregular morphology, is located between the NW caldera and southern cone. The volcano flanks are also characterized by irregular morphologies, which provide evidence of past collapses of different sectors of Rumble III, as given by the asymmetric shapes of the volcano's flanks and the corresponding irregularity in the bathymetric contours [*Grosse et al*., 2009]. A large scar is located on the western flank of Rumble III, beneath the southern cone. This scar has a trapezoidal shape, ~1 km wide at ~400 m water-depth widening to ≥2 km down the volcano western flank, at a water depth ≥2500 m. Prominent ridges are located at the margin and in the center of this scar (Figure 3).

[9] Another, similar scar is located on the NW flank of Rumble III, beneath the NW caldera. Here, the scar is shaped like that of the western scar and is also bordered on its margins by ridges. Both these scars are characterized by smooth morphologies with even contours (Figures 2 and 3) when compared to the rougher morphologies in other flanks of the volcano, characterized by ridge spurs and constructional features. A similar analysis of the bathymetric contours in Figure 2 shows evidence of another potential collapse feature located on the eastern flank of Rumble III, oriented in a NE direction.

[10] These scars provide a geological record of major collapses that have occurred at Rumble III. This is consistent with recent time-series bathymetric surveys showing evidence of significant changes in the volcano shape between 2007 and 2009. In particular, the summit of the southern cone in 2009 was ~100 m deeper in 2009 than it was when mapped in 2007, suggesting a partial collapse of the cone in the intervening period. Furthermore, the NW caldera floor appeared ~20 m shallower in 2009 than in 2007 [*Dodge*, 2010]. Visual exploration using towed camera images show that the caldera floor has been filled with significant ash deposits, providing evidence for a recent eruption [*Dodge*, 2010].

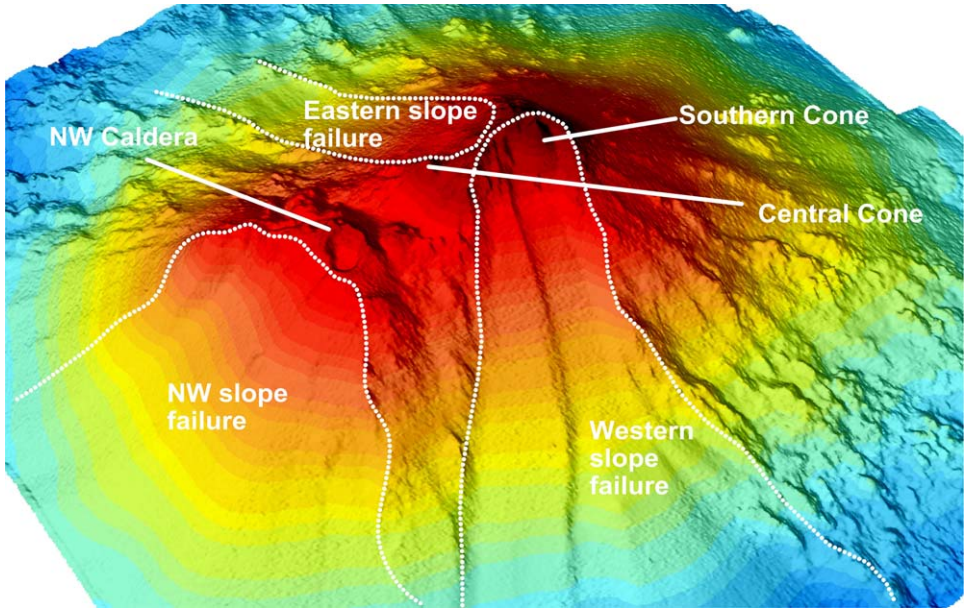

Figure 3. Rumble III 3-D morphology, showing the main volcanic structures (Southern Cone, Central cone, and NW caldera) and past slope failures in the western, NW, and eastern flanks (white dotted lines). Perspective view from NW (see also Figure 2), with vertical exaggeration 2.5×.

[11] Images from towed cameras in selected areas combined with limited rock sampling provide information on the more common Rumble III rock substrates. Fresh and hydrothermally altered basalts and andesites with SiO_2 contents between 50 and 63 wt.% appear to be the major rock composition [*Wright et al*., 2002]. In general, Rumble III flanks are mainly composed of massive lava outcrops, pillow tubes and coarse volcaniclastic sediments showing evidence of gravitational mass-wasting processes [*Wright*, 1994]. Based on the absence (or presence) of comminuted volcaniclastic detrita and effusive eruption products, *Wright et al*. [2002] found a significant change in the substrate type between ~700 m and ~800 m water depth, interpreted to be the transition between effusive and explosive volcanism at Rumble III. More recently, additional substrates were recognized from towed camera images taken during the 2011 NZASMS cruise. These include: talus covering steep slopes, thick ash deposits, and hydrothermal deposits [*Dodge*, 2010].

2.2. Surface Geophysical Data

[12] We carried out gravity and magnetic investigations along the survey lines shown in Figure 2. Accurate ship position was obtained at all times from the ship's DGPS system. The bathymetry data were collected using a Konsberg-Simrad EM300 system and data were processed to obtain a 25 m resolution grid of the seafloor and also a backscatter map (Figure 4a). This map clearly shows some of the volcano flank collapse features discussed in section 2.1 as low-reflectivity regions. Gravity data were collected using a Lacoste & Romberg S-80 dynamic gravity meter. Relative gravity was tied to an absolute station in Auckland harbor before and after the cruise to check for meter drift (~3 mGal/month). Data were corrected for drift and Eotvos effects and processed with a 120 s long Butterworth low-pass filter along the survey lines. The corresponding free-air anomaly is shown in Figure 4b. The complete Bouguer correction was computed with a reference density of 2.4 g/cm^3. This is an optimal value arising from an analysis of the correlation between the gravity anomaly and bathymetry [*Caratori Tontini et al*., 2007] (see also supporting information[1]). The corresponding Bouguer gravity map is shown in Figure 4c.

[13] Magnetic data were collected with a Marine Magnetics Seaspy magnetometer, towed 300 m behind the ship's stern to reduce the magnetic effect of the ship. The data were processed for heading and lag errors, and the anomaly field was obtained by subtracting the 2011 International Geomagnetic Reference Field [*Finlay et al*.,

[1]Additional supporting information may be found in the online version of this article.

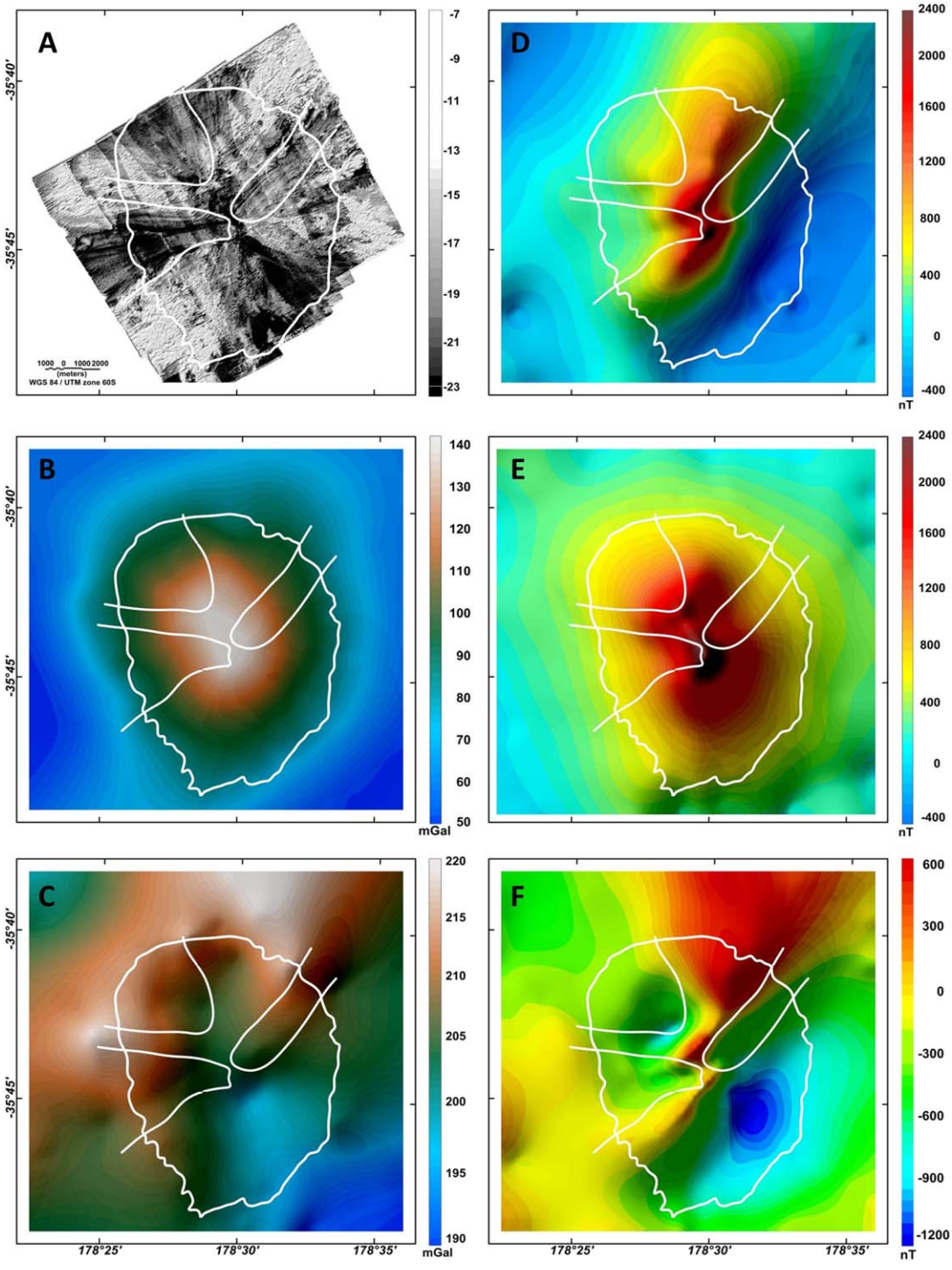

Figure 4. Rumble III surface geophysical maps. White lines represent present-day slope failures in the western, NW, and eastern flanks (see also Figure 3). The white polygon (bathymetry contour at 2000 m) encloses the boundary of Rumble III edifice. (a) EM302 reflectivity map (log scale). Dark areas represent low-reflectivity values. (b) Free-air anomaly map. (c) Complete Bouguer anomaly map, compiled with a reduction density of 2.4 g/cm^3. (d) Total-intensity magnetic anomaly map, reduced to the magnetic pole (ambient geomagnetic field with inclination −60°, declination 20°). (e) Synthetic magnetic anomaly for a 6 A/m uniformly magnetized edifice. (f) Maps of the difference between Figure 4d and 4e.

Table 1. Susceptibility and Magnetization Measurements of Rumble III Samples

Sample	Characteristics	Susceptibility[a]	Magnetization[b]
TC10-1	S Cone, fresh basalt	0.01328	11.2
TC10-2	S Cone, fresh basalt	0.01656	16.6
TC10-3	S Cone, fresh basalt	0.01448	14.2
TC10-4	S Cone, fresh basalt	0.01345	13.2
ES44-1	S Cone, fresh basalt	0.00250	5.6
ES44-2	S Cone, fresh basalt	0.00303	5.2
ES44-3	S Cone, fresh basalt	0.00250	1.9
ES44-4	S Cone, fresh basalt	0.00290	8.1
ES 55	S Cone, fresh basalt	0.00108	11.08
ES51-1	NW caldera, fresh basalt	0.02123	0.84
ES51-2	NW caldera, fresh basalt	0.02217	0.83
ES51-3	NW caldera, fresh basalt	0.02132	0.91
ES51-4	NW caldera, fresh basalt	0.02096	1.77
ES51-5	NW caldera, fresh basalt	0.02006	1.66
ES51-6	NW caldera, fresh basalt	0.02088	1.84
ES51-7	NW caldera, fresh basalt	0.02068	1.62
ES51-8	NW caldera, fresh basalt	0.01942	1.68
TC11-1	S Cone, hydrothermally altered basalt	0.00050	0.24
TC11-2	S Cone, hydrothermally altered basalt	0.00300	1.23
TC11-3	S Cone, hydrothermally altered basalt	0.00086	0.44
ES54-5	S Cone, hydrothermally altered basalt	0.00102	0.67
ES54-6	S Cone, hydrothermally altered basalt	0.00109	0.57

[a]Values in SI, measured with a Bartington MS2 susceptibility meter.
[b]Values in A/m, measured with a Molspin spinner magnetometer.

2010]. We were not able to directly correct for diurnal variations of the magnetic field, as a coherent base station could not be installed close to the survey [*Faggioni and Caratori Tontini*, 2003]. However, analysis of the INTERMAGNET observatory at Eyrewell, near Christchurch (New Zealand), shows that the surveys were performed in magnetically quiet days. Finally, the data have been reduced to the magnetic pole to reduce any skewness effect coming from dipolarity of the magnetic field at midlatitudes. The corresponding anomaly map is shown in Figure 4d. A bulk magnetization estimate for Rumble III was obtained by an approach similar to that used for density estimation, i.e., by reducing the correlation between the observed anomaly and a synthetic anomaly calculated by assuming uniform magnetization. The computation of the synthetic anomaly is based on a 3D-FFT forward modeling algorithm [*Caratori Tontini*, 2012; *Caratori Tontini et al.*, 2009]. We obtained a bulk magnetization of 6 A/m, which generates the synthetic anomaly in Figure 4e. Finally, Figure 4f shows the residual anomaly, i.e., a map of the difference between the observed anomaly and the synthetic anomaly corresponding to a uniform magnetization model of 6 A/m for Rumble III.

[14] The comparison between Bouguer gravity and residual magnetic maps (i.e., Figures 4c and 4f) gives a qualitative understanding of the bulk internal structure of Rumble III, with apparent correlations between the two data sets. In particular, a relatively low-average density of 2.4 g/cm^3 has been found at arc volcanoes in the Tyrrhenian Sea [*Caratori Tontini et al.*, 2010]. A bulk magnetization of 6 A/m is also compatible with the relatively large spectrum of magnetization measurements derived from submarine arc volcanoes basalts and andesites [*Carmichael*, 1982]. In addition, we have performed susceptibility and magnetization measurements on a limited number of rock samples dredged from Rumble III. The results are summarized in Table 1; the preference of 6 A/m magnetization is in reasonable agreement with these measurements.

[15] Both gravity and magnetic measurements provide evidence of large-scale density and magnetization variations in the internal structure of Rumble III. In particular, the SE flank (see Figure 4c) is characterized by a gravity low that may be caused by the presence of low-density rocks. Similarly, a prevalent magnetic low is also present in this region (Figure 4f). Thus, the SE sector of the volcano is characterized by low-density and low-magnetization rocks. In addition, backscatter data (-Figure 4a) show a coincident low-reflectivity region, indicating less consolidated material. Another feature common to both Bouguer gravity and residual magnetic maps are the triangular-shaped gravity and magnetic anomalies, N-S oriented, extending along the northern flank of Rumble III. Both of these anomalies are located between the NW and E scars (Figures 2 and 3), delimited by the same ridge features which border the scars.

[16] Figure 4f also shows that the ridge bordering the southern side of the western scar is characterized by a linear positive magnetic anomaly. Similarly, the summit region between the southern cone and the NW caldera is characterized by a linear high magnetic anomaly. By contrast, the western and NW failures are instead characterized by low magnetic anomalies, similarly to the SE flank.

2.3. Near-Seafloor Geophysical Data

[17] The summit region of Rumble III was surveyed in detail during two dives with the AUV *Sentry*. The survey lines are shown in Figure 5a. The data were collected at an average constant

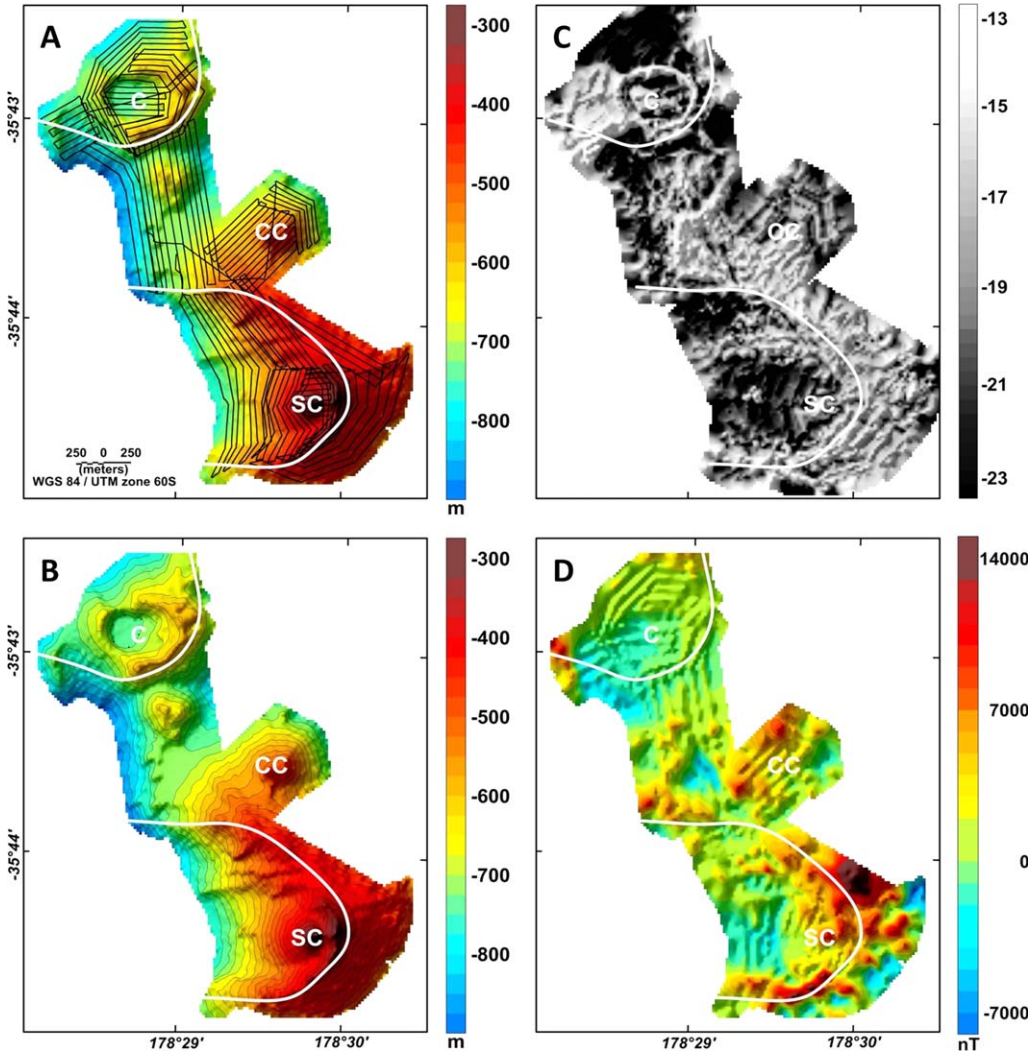

Figure 5. Rumble III AUV-derived (*Sentry*) geophysical maps. (a) *Sentry* survey lines. White lines represent present-day slope failures in the western and NW sectors. C is the NW caldera, CC is the central cone, and SC is the South cone. (b) Detailed bathymetry of the edifice summit surveyed by *Sentry*. Contour lines every 25 m. (c) *Sentry* sidescan image (reflectivity). (d) Total-intensity magnetic anomaly map, reduced to the magnetic pole under the same parameters used in Figure 4d.

elevation of ~30 m above the seafloor. The average line spacing was ~50 m. Figure 5b shows the bathymetry map of the survey region. Figure 5c shows the reflectivity map obtained by processing the sidescan sonar data recorded by *Sentry*. The magnetic data were collected using a three axis Honeywell HMR2300 digital magnetometer. The raw vector data were transformed into a total-intensity field and corrected for the magnetic noise generated by the AUV. This correction is calculated by fitting the variation of the magnetic field while the AUV spins during its descent to the seafloor [*Tivey et al.*, 2003; *Caratori Tontini et al.*, 2012a]. These data were then corrected according to the standard procedure described above for surface magnetic data. The resulting magnetic anomaly map is shown in Figure 5d.

[18] The western failure is defined by a region of low-magnetic anomaly, delimited by a linear positive anomaly coincident with the flank ridges. The sidescan image also provides evidence of low-reflectivity rocks in these regions. The southern cone is identified by a large, positive magnetic anomaly and by a largely reflective substrate. The NW caldera is characterized by low-magnetic anomalies. However, the caldera walls appear to have relatively bright reflectivity when compared to the caldera floor. This is consistent with the findings by *Dodge* [2010] who noted a thick layer of ash filling the caldera floor.

3. Rumble III 3-D Magnetic Model

[19] We use the magnetic data to infer a 3-D magnetization model of Rumble III. This is an important constraint to assess weak zones at Rumble III. We consider and discuss the 3-D magnetization model as a first-order geophysical expression of the subsurface rock distribution. The magnetization model is then correlated with other geophysical data to assess weak regions at Rumble III.

3.1. Correlation Between Magnetization Model and Rock Properties

[20] We discussed above the relevant role played by hydrothermal alteration in weakening volcanic rocks. We know that fresh volcanic rocks, and basalts in particular, are characterized by large magnetizations. However, it is also well known that hydrothermal fluid circulation can drastically decrease the host rock magnetizations in both submarine hydrothermal systems [*Johnson and Atwater*, 1977; *Rona*, 1978; *Tivey and Johnson*, 2002; *Tivey and Dyment*, 2010]. Magnetic data can thus provide important information on the distribution of relatively fresh (strong) and hydrothermally altered (weak) rocks [*Reid et al*., 2001; *Finn et al*., 2001; *Caratori Tontini et al*., 2010]. In particular, hydrothermally altered zones in the volcano subsurface are characterized by widespread low-magnetization regions.

[21] It is possible that other substrates could be responsible for low-magnetization anomalies at Rumble III, other than hydrothermal alteration. Ash, for example, is characterized by a reduced magnetite content. The chaotic redistribution of pyroclastic and volcanoclastic material can also break up any large-scale correlation in the remanent magnetization distribution. This may also contribute to explain the presence of low-magnetization anomalies in regions where failures have already occurred, because these regions may be characterized by volumes of volcanic debris from previous flank collapses.

[22] It is difficult to distinguish between a scenario of hydrothermally altered rocks or variable substrate from analysis of geophysical data alone. However, these alternative scenarios can be still characterized by reduced rock strength. For example, poorly consolidated material, such as pyroclastics, volcanoclastics, and ash deposits may be characterized by reduced rock strength relative to fresh basalts. As we will discuss in the following, backscatter and sidescan data (Figures 4a and 5c) highlight areas of low-reflectivity coincident with areas of low magnetization, suggesting the presence of less consolidated material. Understanding the possible limits imposed by these assumptions, we use the subsurface magnetization model to assess the 3-D model of rock distribution for Rumble III, assuming that low-magnetization anomalies highlight the presence of weak rocks in areas that do not appear to have experienced past slope failures.

3.2. 3-D Magnetic Model: Inversion of Magnetic Anomalies

[23] To obtain the subsurface magnetization distribution, we applied a quantitative inversion algorithm to the magnetic anomalies. The inversion is a mathematical process used to find a subsurface 3-D magnetization distribution which reproduces the magnetic observations. The common parameterization of the inversion process is based on subdividing the Earth's subsurface (subseafloor) into a 3-D grid of smaller juxtaposed prismatic cells each characterized by a constant magnetization value. The inversion is aimed at determining the magnetization of these cells so that complex 3-D magnetization distributions can be obtained. This process is characterized by nonuniqueness and ambiguities of the solution. In order to reduce these ambiguities, constraints about the source geometry are introduced in the inversion process. This gives a magnetization distribution subject to fitting the observations and satisfying some basic geological information regarding the shape of the distribution and the range of the magnetization parameters.

[24] For the Rumble III magnetic data, we have applied the inversion method given in *Caratori Tontini et al*. [2012b], where the mathematical details of the inversion are discussed. Here we summarize the basic constraints:

[25] 1. The magnetization direction is assumed to be parallel to the ambient geomagnetic field. For Rumble III, the magnetization direction is characterized by inclination of −60° and declination 20°.

[26] 2. The magnetization values are forced to lie within a predetermined range, i.e., lower and upper bounds on the magnetization values are used. The imposed range of magnetization for Rumble III is [0–6] A/m, based on the correlation between bathymetry and magnetic maps shown in Figure 4 (see also supporting information). We impose positive magnetization values because Rumble III is younger than the last geomagnetic polarity reversal.

[27] 3. A sharp, focused solution is found by minimizing the volume of the regions where the gradient of the magnetization distribution is significantly different from zero.

[28] These constraints are introduced to select a specific solution among the set of possible solutions fitting the observations within the same degree of accuracy. In particular, due to the nonuniqueness of potential-field data interpretation there are trade-offs between volumes, depths and intensity of the magnetization distribution. However, the horizontal resolution of the inversion model is not particularly sensitive to these parameters. The choice of a particular range of magnetization and the minimum volume constraint discussed above characterize the ambiguity domain of our inversion algorithm. Thus, care should be taken when analyzing the magnetization model to extract quantitative information, as different constraints may give different magnetization distributions.

[29] However, if our geological interpretation in terms of hydrothermal alteration is correct, our constraints should be particularly effective because we expect to have sharp contacts between hydrothermally altered zones and fresh volcanic rocks [*Caratori Tontini et al*., 2012b]. Furthermore, our minimum volume constraint may be give conservative results, as minimum values are obtained for the nonmagnetic regions at Rumble III, implying a possible underestimation of the real thicknesses and sizes of the corresponding weak zones. However, before discussing our model it is important to understand its limitations as the adopted constraints may not be fully representative of the complex geology of Rumble III.

[30] We performed the inversion in two steps. First, we inverted the AUV data (Figure 5d), and obtained a 3-D magnetization model for the top portion of Rumble III, i.e., down to a depth of ~1000 m. Then, we inverted the surface magnetic data (Figure 4d), to obtain a lower resolution 3-D magnetization model for Rumble III volcano, down to a depth of ~2000 m. The two models were then merged into a composite model, composed of lower resolution (surface data) magnetization model in the depth range [1000–2000] m, and high-resolution (AUV) magnetization model in the depth range [200–1000] m (see supporting information for a 3-D volume interactive representation using a set of magnetization isosurfaces).

3.3. 3-D Magnetic Model: Interpretation for the Rock Properties

[31] The surface expression of the 3-D magnetization model and its interpretation in terms of rock strength is shown in Figure 6, viewed from different directions. In this figure, low-magnetization regions (weak rocks) are blue, whereas high-magnetization regions (strong rocks) are red. The thicknesses of these different rock types can be extrapolated from the interactive 3-D magnetization model shown in supporting information. All the known slope failures at Rumble III have been highlighted by white lines in Figure 6 and show a good correlation with the presence of low-magnetization anomalies, especially near the summit of the volcano, or the head of the scars, in particular at the W flank and NW flank failures. The magnetization results are also in good agreement with the back-scatter data shown in Figure 4a. These regions are characterized by low-reflectivity, indicating poorly consolidated substrates. Hydrothermal venting and hydrothermally altered rocks have been observed in these regions, at depth shallower than ~1000 m, indicating that weak rocks from hydrothermal alteration may be the primary cause for collapses of these sectors, at least in their summit regions.

[32] The more relevant result of the magnetization model is a wide region of potentially weak rocks, i.e., the SE flank (Figure 6d). Here, a ~1.5 km wide substrate of low-magnetization extends from the volcano summit down to the volcano base, widening to ~5 km at a water depth > 1500 m. This region correlates with a low-reflectivity and low-density region (Figures 4a and 4c). The bathymetry map (Figures 2 and 3) does not provide clear evidence of existing slope failures in this region. Here, post-eruption hydrothermal alteration of the basalts may still explain the observed low magnetization. However, the presence of a relative low in the gravity anomaly, not observed in other parts of Rumble III, and the apparent absence of preexisting seafloor failures in this region suggest that differences in the rock substrate can also provide a possible explanation for this observation. In particular, depending on the viscosity of the melt during the eruption and on eruption rate, hyaloclastites may be the relevant products of submarine eruptions [*Bonatti and Harrison*, 1988]. The presence of hyaloclastites could explain the observed low gravity and magnetic anomaly in this region, because these rocks typically have low densities and magnetizations. Additional data, in particular dredges and towed camera observations are needed to prove this speculation. However, if the presence of hyaloclastites is the explanation for our observations, the corresponding region is again characterized by weak rocks that may promote further collapses [*Schiffmann et al*., 2006; *Caratori Tontini et al*., 2010].

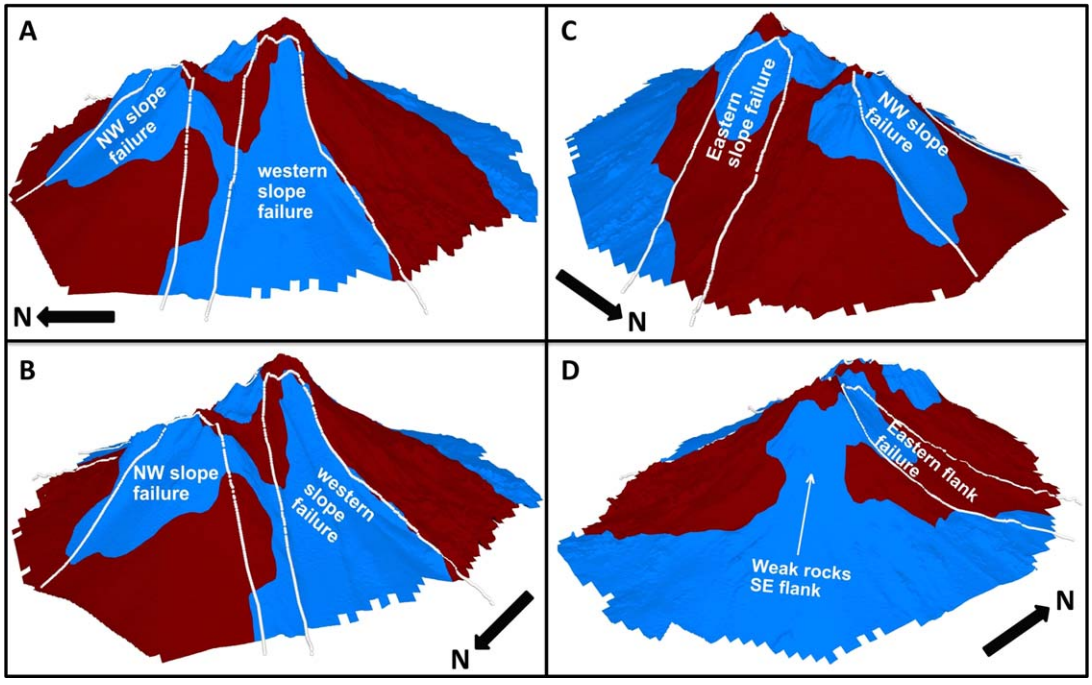

Figure 6. Surface expression of Rumble III 3-D magnetization model. Blue areas represent low magnetizations ([0–3] A/m), interpreted as weak rocks. Red areas represent large magnetization ([3–6] A/m), interpreted as strong rocks. White lines represent present-day slope failures in the western, NW and eastern flanks (see also Figure 3). (a) Perspective view from West. (b) Perspective view from NW. (c) Perspective view from NE. (d) Perspective view from SE. The low-magnetization region (interpreted as weak rocks on the SE flank) is also highlighted. This regions does not show any apparent correlations with past slope failures.

4. Discussion

[33] Backscatter and magnetic anomalies (Figures 4a and 4f) show some interesting correlations with apparent past slope failures, particularly at the NW and western sectors. The 3-D magnetization model shown in Figure 6 provide further evidence of this correlation, where low-magnetization regions are observed in the regions affected by past failures. It is difficult to understand if these low-magnetization anomalies may indicate high failure potential for these regions, as it is possible that past failures might have entirely removed the weaker materials, and/or redeposited them into more stable configurations. If this is the case, the magnetization and backscatter anomalies can be caused, at least at greater depths ($\geq$1000 m), by the chaotic redistribution of debris coming from previous landslides. This would break any large-scale correlation in the remanent magnetization distribution, leaving a small-induced contribution. However, even taking into account its limits, the 3-D magnetization model provides evidence that the thicknesses of these regions are quite large, $\sim$500 m under the eastern slope failure and up to $\sim$1000 m below the western and NW slope failures (see supporting information).

[34] Due to ambiguities in the inversion process, these numbers may be rough approximation, however we cannot exclude the presence of weak rocks underneath the thin debris layer which may promote further flank collapses. The removal of weaker materials subject to failure might have modified the stratigraphy, both compositional and mechanical, of shallow slopes, exposing poorly magnetized rocks that differ from the surrounding areas. Furthermore, in the case of a substrate dominated by hydrothermally altered rocks, flank collapses may open new pathways for the upflow of hydrothermal fluids and subsequent hydrothermal alteration of volcanic rocks after the failure. In effects, the time scale of hydrothermal alteration is short relative to the recurrence time of submarine volcanoes flank collapses [*Lowell et al.*, 1995], i.e., there is enough time for hydrothermal alteration to occur in areas that have experienced past slope failures. Additional observations are needed in order to assess high failure potentials in these regions already affected by past collapses.

[35] The most interesting part of Rumble III, relative to sector collapse, is the SE flank (Figure 6d). This is an area that does not appear to have experienced past slope failures, but might consist of weak material capable of future failures. This region in effect is characterized by a strong correlation between gravity (Figure 4c) and magnetic anomalies (Figure 4f), highlighting the existence of a significant volume of low density, poorly magnetized material. In addition, low reflectivity from backscatter data (Figure 4a) also suggests the same area is characterized by poorly consolidated material.

[36] The low-density anomaly is a significant difference between the geophysical signatures of the SE flank relative to other regions characterized by past slope failures, where the corresponding gravity map does not show a clear negative anomaly. As discussed in the previous section, this difference might be explained in terms of different rock substrates in this region, as for example hyaloclastites. However, it is possible that past failures at Rumble III might have involved similar substrates of low-density rocks, and possibly have swept away these materials, exposing rocks characterized by higher densities. This hypothesis may imply low failure potential in regions characterized by past collapses, but higher failure potential for the SE flank.

[37] Understanding the uncertainties and possible limitations, the 3-D magnetization model (Figure 6, see also supporting information) may be used to estimate the size and volumes of a potential failure of the SE flank of Rumble III. The top portion of the demagnetized region is $\sim$1.5 km wide and extends to depths $>$ 2 km, with a maximum thickness of $\sim$200 m. If our interpretation is correct, this implies a significant volume of $\sim$0.7 km^3 of potentially weak rocks at relatively shallow depth. In order to understand if the failure of the SE flank may be relevant in terms of tsunami hazard, we estimate the approximate amplitude of potential tsunami triggered by these collapses. We base these discussions on the tsunami generation model discussed by *Grilli et al*. [2009], which is aimed at determining an initial tsunami characteristic amplitude η_0, or the maximum depression of the ocean surface above the center of the submarine landslide [*Grilli and Watts*, 2005; *Watts et al*., 2005].

[38] In particular, a failure of the SE flank of Rumble III, occurring in a single event, could generate a wave with an amplitude $\eta_0 \sim 11$ m. It is important to remember that these numbers are only rough approximations, and error estimates for the previous η_0 values can be as large as $\pm$50%. Furthermore, the amplitude of this wave would decrease quickly away from the source. Nevertheless, the rise of bathymetry close to coast of New Zealand could enhance again the amplitude of this wave. A detailed calculation of the tsunami generation model is beyond the scope of this paper, however these findings suggest that major flank failures at Rumble III may be capable of generating significant tsunami.

5. Conclusions

[39] We have collected and interpreted shipborne and near-seafloor geophysical data at Rumble III submarine volcano to understand the hazard associated with potential flank failures. Backscatter and magnetic anomalies show an interesting correlation with past flank failures at Rumble III, that may be partially explained by the presence of nonmagnetic and poorly consolidated debris from previous collapses. Based on geophysical data only, we cannot exclude that further collapses may occur in these areas. Based on inversion of magnetic data, we obtained a 3-D model of the magnetization distribution that we used to define potential sizes and locations of weak zones at Rumble III. As magnetization is strongly reduced in poorly consolidated materials and in the presence of hydrothermal alteration, we have interpreted low-magnetization regions as a first-order approximation of weak regions at Rumble III that may promote future collapses.

[40] Possible exceptions may limit the validity of this model, as ambiguities in the inversion solution may affect the estimated sizes and extent of the low-magnetization regions. Furthermore, in some settings as Hawaii, volcanoclastic rocks with low magnetizations have proven to have higher mass strength than highly magnetic basalts because of cementation. However, in the vast majority of cases a correlation exist between reduced rock strength and low magnetization. In particular, weak rocks as hyaloclastites may also be characterized by low magnetizations and may explain the widespread gravity anomaly observed at the SE flank. This is the most interesting part of Rumble III in terms of high failure potential, because it is a region that does not appear to have experienced past slope failures, but might consist of $\sim$0.7 km^3 of weak rocks capable of promoting future failures with possible associated tsunami.

[41] At intraplate volcanic islands and seamounts dominated by basaltic composition, such as Hawaii and the Canary islands, volcano destruction is dominated by large and infrequent collapses [*Moore et al.*, 1989; *Masson*, 1996; *McGuire*, 2006], whereas active arc volcanoes show that small scale, more frequent landslides may be a more relevant mass-wasting process [*Lindsay et al.*, 2005; *Chadwick et al.*, 2005; *Wright et al.*, 2006, 2008]. At Rumble III, there is evidence for existing failures at different spatial scales [*Dodge*, 2010] with thicknesses ranging from ~10 m, likely to be related to more frequent and intermittent mass-wasting processes related with volcanic activity and eruption processes [*Wright et al.*, 2006], up to ~100–200 m, such as the noneruptive sector collapse of the western flank, that was likely to have occurred in a single event.

[42] To date, there is no clear evidence of tsunami, or deposits formed by tsunami, in New Zealand that was generated by sector collapse of submarine volcanoes in the Kermadec arc. A possible exception is the correlation between the inferred collapse of the Healy caldera (located ~200 km NE of Rumble III) and pumice deposits found in northern areas of New Zealand [*Wright and Gamble*, 1999; *Wright et al.*, 2003; *Nichol et al.*, 2003]. However, our analysis at Rumble III has shown that large portions of the edifice might be characterized by weak rocks, and they have the potential to cause large collapses that may trigger tsunami with amplitudes on the order of 10 m. Geophysical models may greatly increase the accuracy of any stability assessment of submarine volcanoes, showing that this is a useful approach when deciphering hazard prediction.

Acknowledgments

[43] The paper has greatly benefited from the review by Richard J. Blakely and an unknown reviewer. We thank the crews of the R/V *Tangaroa* for the safe deployment and recovery of the AUV *Sentry*. We also thank Andy Billings, Alan Duester, and Carl Kaiser from WHOI for the successful operation of *Sentry*. The magnetization and susceptibility measurements were made thanks to Christian Onheiser, Gary Wilson, and Claudio Tapia at the University of Otago Paleomagnetic Research Facility. This contribution was funded by the Royal Society of New Zealand by the Marsden Fund (grant GNS1003).

References

Baker, E. T., R. A. Feely, C. E. J. de Ronde, G. J. Massoth, and I. C. Wright (2003), Submarine hydrothermal venting on the southern Kermadec volcanic arc front (offshore New Zealand): Location and extent of particle plume signatures, *Geol. Soc. Spec. Publ.*, *219*, 141–161.

Bjornsson, A., L. Kristjansson, and H. Johnsen (1976), Some observations of the Heimaey deep drill hole during the eruption of 1973, *Jokull*, *26*, 52–57.

Bonatti, E., and C. Harrison (1988), Eruption styles of basalts in oceanic spreading ridges and seamounts: Effects of magma temperature and viscosity, *J. Geophys. Res.*, *93*, 2967–2980.

Caratori Tontini, F. (2012), Rapid interactive modeling of 3D magnetic anomalies, *Comput. Geosci.*, *48*, 308–315, doi:10.1016/j.cageo.2012.01.006.

Caratori Tontini, F., F. Graziano, L. Cocchi, C. Carmisciano, and P. Stefanelli (2007), Determining the optimal Bouguer density for a gravity data set: Implications for the isostatic setting of the Mediterranean Sea, *Geophys. J. Int.*, *169*, 380–388.

Caratori Tontini, F., L. Cocchi, and C. Carmisciano (2009), Rapid 3-D forward model of potential fields with application to the Palinuro Seamount magnetic anomaly (Southern Tyrrhenian Sea, Italy), *J. Geophys. Res.*, *114*, B02103, doi:10.1029/2008JB005907.

Caratori Tontini, F., L. Cocchi, F. Muccini, C. Carmisciano, M. Marani, E. Bonatti, M. Ligi, and E. Boschi (2010), Potential-field modeling of collapse-prone submarine volcanoes in the southern Tyrrhenian Sea (Italy), *Geophys. Res. Lett.*, *37*, L03305, doi:10.1029/2009GL041757.

Caratori Tontini, F., B. Davy, C. E. J. de Ronde, R. W. Embley, M. Leybourne, and M. A. Tivey (2012a), Crustal magnetization of Brothers volcano, New Zealand, measured by autonomous underwater vehicles: Geophysical expression of a submarine hydrothermal system, *Econ. Geol.*, *107*, 1571–1581.

Caratori Tontini, F., C. E. J. de Ronde, D. Yoerger, J. C. Kinsey, and M. A. Tivey (2012b), 3-D focused inversion of near-seafloor magnetic data with application to the Brothers volcano hydrothermal system, Southern Pacific Ocean, New Zealand, *J. Geophys. Res.*, *117*, B10102, doi:10.1029/2012JB009349.

Carmichael, R. S. (1982), Magnetic properties of minerals and rocks, in *Handbook of Physical Properties of Rocks*, edited by R. S. Carmichael, pp. 229–287, CRC Press, Boca Raton, Fla.

Chadwick, W. W., Jr., R. W. Embley, P. D. Johnson, S. G. Merle, S. Ristau, and A. Bobbit (2005), The submarine flanks of Anatahan Volcano, commonwealth of the Northern Mariana Islands, *J. Volcanol. Geotherm. Res.*, *146*, 8–25.

Day, S. J. (1996), Hydrothermal pore fluid pressure and the stability of porous, permeable volcanoes, Volcano Instability on the Earth and Other Planets, *Geol. Soc. Spec. Publ.*, *110*, 77–93.

DeMets, C., R. G. Gordon, and D. F. Argus (2010), Geologically current plate motions, *Geophys. J. Int.*, *181*, 1–80.

de Ronde, C. E. J., E. T. Baker, G. J. Massoth, L. E. Lupton, I. C. Wright, R. A. Feely, and R. G. Greene (2001), Intra-oceanic subduction-related hydrothermal venting, Kermadec volcanic arc, New Zealand, *Earth Planet. Sci. Lett.*, *193*, 359–369.

Dodge, E. (2010), Catastrophic volcanic activity at Rumble III Volcano based on EM300 bathymetry and direct sea floor imaging, Senior thesis for Oceanography 444, Univ. of Washington, Sch. of Oceanogr., Seattle, Wash.

Elsworth, D., and B. Voight (1995), Dike intrusion as a trigger for large earthquakes and the failure of volcano flanks, *J. Geophys. Res.*, *100*, 6005–6024.

Faggioni, O., and F. Caratori Tontini (2003), Quantitative evaluation of the time-line reduction performance in high definition marine magnetic surveys, *Mar. Geophys. Res.*, *23*, 353–365.

Finlay, C. C., et al. (2010), International geomagnetic reference field: The eleventh generation, *Geophys. J. Int.*, *183*, 1216–1230.

Finn, C. A., T. W. Sisson, and M. Deszcz-Pan (2001), Aerogeophysical measurements of collapse-prone hydrothermally altered zones at Mount Rainier volcano, *Nature*, *409*, 600–603.

Grilli, S. T., and P. Watts (2005), Tsunami generation by submarine mass failures. I: Modeling, experimental validation, and sensitivity analyses, *J. Waterw. Port Coastal Ocean Eng.*, *131*, 283–297.

Grilli, S. T., O-D. S. Taylor, C. D. P. Baxter, and S. Maretzki (2009), A probabilistic approach for determining submarine landslide tsunami hazard along the upper east coast of the United States, *Mar. Geol.*, *264*, 74–97.

Grosse, P. B., B. van Wyk de Vries, I. A. Petrinovic, P. A. Euillades, and G. E. Alvarado (2009), Morphometry and evolution of arc volcanoes, *Geology*, *37*, 651–654.

Jaeger, J. C., and N. G. W. Cook (1979), *Fundamentals of Rock Mechanics*, Chapman and Hall, New York.

Johnson, H. P., and T. Atwater (1977), Magnetic study of basalts from the mid-Atlantic ridge, lat. 37°N, *Geol. Soc. Am. Bull.*, *88*, 637–647.

Latter, J. H., E. F. Lloyd, I. E. M. Smith, and S. Nathan (1992), Volcanic hazards in the Kermadec Islands, and at submarine volcanoes between Southern Tonga and New Zealand, *Volcan. Hazard Inf. Ser.*, *4*, 1–43.

Lindsay, J. M., J. B. Shepherd, and D. Wilson (2005), Volcanic and scientific activity at Kick'em Jenny submarine volcano 2001–2002: Implications for volcanic hazards in the southern Grenadines, Lesser Antilles, *Nat. Hazards*, *34*, 1–24.

Lopez, D. L., and S. N. Williams (1993), Catastrophic volcano collapse; relation to hydrothermal processes, *Science*, *260*, 1794–1796.

Lowell, R. P., P. A. Rona, and R. P. Von Herzen (1995), Seafloor hydrothermal systems, *J. Geophys. Res.*, *100*, 327–352.

Masson, D. G. (1996), Catastrophic collapse of the flank of El Hierro about 15000 years ago, and the history of large flank collapses in the Canary Islands, *Geology*, *24*, 231–234.

Massoth, G. J., C. E. J. de Ronde, J. E. Lupton, R. A. Feely, E. T. Baker, G. T. Lebon, and S. M. Maenner (2003), Chemically rich and diverse submarine hydrothermal plumes of the southern Kermadec volcanic arc (New Zealand), *Geol. Soc. Spec. Publ.*, *219*, 119–139.

McGuire, W. J. (1996), Volcano instability: A review of contemporary themes, *Geol. Soc. Spec. Publ.*, *110*, 1–23.

McGuire, W. J. (2006), Lateral collapse and tsunamigenic potential of marine volcanoes, *Geol. Soc. Spec. Publ.*, *269*, pp. 1–23.

Moore, J. G., D. A. Clague, R. T. Holcomb, P. W. Lipman, W. R. Normark, and M. E. Torresan (1989), Prodigious submarine landslides on the Hawaiian ridge, *J. Geophys. Res.*, *94*, 17,465–17,484.

Nichol, S. L., O. B. Lian, and C. H. Carter (2003), Sheet-gravel evidence of a late Holocene tsunami run-up on beach dunes, Great Barrier Island, New Zealand, *Sediment. Geol.*, *155*, 129–145.

Reid, M. E. (2004), Massive collapse of volcano edifices triggered by hydrothermal pressurization, *Geology*, *32*, 373–376.

Reid, M. E., T. W. Sisson, and D. L. Brien (2001), Volcano collapse promoted by hydrothermal alteration and edifice shape, Mount Rainier, Washington, *Geology*, *29*, 779–782.

Rona, P. A. (1978), Magnetic signatures of hydrothermal alteration and volcanogenic mineral deposits in oceanic crust, *J. Volcanol. Geotherm. Res.*, *3*, 219–225.

Schiffmann, P., R. J. Watters, N. Thompson, and A. W. Walton (2006), Hyaloclastites and the slope stability of Hawaiian volcanoes: Insights from the Hawaiian Scientific Drilling Projects's 3-km drill core, *J. Volcanol. Geotherm. Res.*, *151*, 217–228.

Siebert, L., H. Glicken, and T. Ui (1987), Volcanic hazards from Bezymianny- and Bandai-type eruptions, *Bull. Volcanol.*, *49*, 435–459.

Sillitoe, R. H. (1985), Ore-related breccias in volcanoplutonic arcs, *Econ. Geol.*, *80*, 1467–1514.

Smith, M. S., and J. B. Shepherd (1996), Tsunami waves generated by volcanic landslides: An assessment of the hazard associated with Kick'em Jenny, Volcano Instability on the Earth and Other Planets, *Geol. Soc. Spec. Publ.*, *110*, 115–123.

Tivey, M. A., and J. Dyment (2010), The magnetic signature of hydrothermal systems in slow spreading environments, in *Diversity of Hydrothermal Systems on Slow Spreading Ocean Ridges, Geophys. Monogr. Ser.*, vol. *188*, edited by P. Rona, C. Devey, and B. Murton, pp. 43–65, AGU, Washington, D. C.

Tivey, M. A., and H. P. Johnson (2002), Crustal magnetization reveals subsurface structure of Juan de Fuca Ridge hydrothermal vent fields, *Geology*, *30*, 979–982.

Tivey, M. A., H. Schouten, and M. C. Kleinrock (2003), A near-bottom magnetic survey of the Mid-Atlantin Ridge axis at 26°N: Implications for the tectonic evolution of the TAG segment, *J. Geophys. Res.*, *108*(B5), 2277, doi:10.1029/2002JB001967.

Voight, B., R. H. Janda, H. Glicken, and P. M. Douglas (1983), Nature and mechanics of the Mount St. Helens rockslide-avalanche of 18 May 1980, *Geotechnique*, *33*, 243–273.

Watanabe, H. (1983), Changes in water level and their implications to the 1977–1978 activity of Usu volcano, in *Arc Volcanism: Physics and Tectonics*, edited by D. Shimozoru and I. Yokohama, pp. 81–93, Terra Sci., Tokyo.

Watters, R. J., and W. D. Delahaut (1995), Effect of argillic alteration on rock mass stability, *Rev. Eng. Geol.*, *X*, 139–150.

Watters, R. J., D. R. Zimbelman, S. D. Bowman, and J. K. Crowley (2000), Rock mass strength assessment and significance to edifice stability: Mount Rainier and Mount Wood, Cascade Range Volcanoes, *Pure Appl. Geophys.*, *157*, 957–976.

Watts, P., S. T. Grilli, J. T. Kirby, D. R. Tappin, and G. J. Fryer, (2005), Tsunami generation by submarine mass failures. II: Predictive equations and case studies, *J. Waterw. Port Coastal Ocean Eng.*, *131*, 298–310.

Wright, I. C. (1994), Nature and tectonic setting of the Southern Kermadec submarine arc volcanoes: An overview, *Mar. Geol.*, *118*, 217–236.

Wright, I. C., and J. A. Gamble (1999), Southern Kermadec submarine caldera arc volcanoes (SW Pacific): Caldera formation by effusive and pyroclastic eruption, *Mar. Geol.*, *161*, 207–227.

Wright, I. C., J. A. Gamble, and P. A. Shane (2003), Submarine, silicic volcanism of the Healy caldera, southern Kermadec arc (SW Pacific): I, volcanology and eruption mechanism, *Bull. Volcanol.*, *65*, 15–29.

Wright, I. C., P. Stoffers, M. Hannington, C. E. J. de Ronde, P. Herzig, I. E. M. Smith, and P. R. L. Browne (2002), Towed-camera investigations of shallow-intermediate water-depth submarine stratovolcanoes of the Southern Kermadec arc, New Zealand, *Mar. Geol.*, *185*, 207–218.

Wright, I. C., T. J. Worthington, and J. A. Gamble (2006), New multibeam mapping and geochemistry of the 30°–35° sector, an overview of southern Kermadec arc volcanism, *J. Volcanol. Geotherm. Res.*, *149*, 263–296.

Wright, I. C., W. C. Chadwick, Jr., C. E. J. de Ronde, D. Reymond, O. Hyvernaud, H.-H. Gennerich, P. Stoffers, K. Mackay, M. A. Dunkin, and S. C. Bannister (2008), Collapse and reconstruction of Monowai submarine volcano, Kermadec arc, 1998–2004, *J. Geophys. Res.*, *113*, B08S03, doi:10.1029/2007JB005138.